

Generation of runaway electrons and X rays in an inhomogeneous electric field at high gas pressures

V.F. TARASENKO,^{1,2,3} E.Kh. BAKSHT,¹ D.V. BELOPLOTOV,^{1,2} A.G. BURACHENKO,^{1,2}
M.I. LOMAEV,^{1,2} AND D.A. SOROKIN¹

¹Institute of High Current Electronics, Tomsk 634055, Russia

²National Research Tomsk State University, Tomsk 634050, Russia

³National Research Tomsk Polytechnic University, Tomsk 634050, Russia

(RECEIVED 11 September 2016; ACCEPTED 10 October 2016)

Abstract

Results of experimental studies of the amplitude–temporal characteristics of a runaway electron (RE) beam, as well as breakdown voltage and discharge current with a picosecond time resolution are presented. The maximum pressure, at which a RE beam is detectable, decreases with increasing the voltage rise time. The waveforms of the discharge and RE beam currents are synchronized with those of the voltage pulses. It is shown that the amplitude–temporal characteristics of the RE beam depend on the designs of the gas-filled diode and cathode, as well as the gap length. The mechanism for the generation of REs in atmospheric-pressure gases is analyzed on the basis of the obtained experimental data.

Keywords: Gas-filled diode; High pressure; Runaway electrons; Subnanosecond breakdown; Supershort avalanches electron beam; SAEB

1. INTRODUCTION

The generation of runaway electrons (REs) and X-rays is a fundamental physical phenomenon in high-pressure pulsed discharges. The possibility of REs arising in the Earth atmosphere was predicted by Professor Wilson as far back as 1924 (Wilson, 1924) and only 42 years later the prediction was proven by laboratory experiments (Frankel *et al.*, 1966): X rays were detected in pulsed discharges in atmospheric-pressure helium at applying voltage pulses of a negative polarity with an amplitude of tens of kilovolts to a point-to-plane gap. It was shown that for the generation of REs at atmospheric pressure, the gap design should provide an inhomogeneous electric field distribution (by using a cathode with a small radius of curvature) (Frankel *et al.*, 1966). Another pioneering study (Stankevich & Kalinin, 1967) showed the presence of X rays in pulsed discharges in atmospheric-pressure air at both polarities of applied nanosecond voltage pulses. Later, both X-ray emission and RE beam were detected in atmospheric-pressure air and other gases (Tarasova & Khudyakova, 1969; Tarasova *et al.*, 1974).

REs generation in high-pressure gases is a fundamental physical phenomenon resulting, in particular, in the formation of a diffuse discharge without an external ionizing source providing preliminary gas ionization (preionization) (Tarasova *et al.*, 1974; Babich, 2003; Yakovlenko, 2007; Tarasenko *et al.*, 2008a; Levko *et al.*, 2012; Tarasenko, 2014). To date, there are several hundred publications on the generation of RE beams and X-ray emission in laboratory discharges at atmospheric pressure [see monograph (Babich, 2003), collection of papers (Yakovlenko, 2014), collective monograph (Tarasenko, 2014), reviews (Tarasenko *et al.*, 2008a; Levko *et al.*, 2012), and references therein]. However, the results obtained in different research groups differ substantially. In addition, new works are dedicated to the rectification of old results. For example, in (Tarasova & Khudyakova, 1969) REs prints on an X-ray film were interpreted as X-ray ones. It led to an overestimation of the number of X-ray photons. Only in the subsequent work (Tarasova *et al.*, 1974) of those authors, an RE beam in atmospheric-pressure air was detected using a Faraday cup.

There are various reasons for the difference in the results of RE studies obtained by different authors. First, the duration of the RE beam is very short ($\sim 10^{-10}$ s) and depends on the experimental conditions, that lead to difficulties in correct measurements of the amplitude and duration of the

Address correspondence and reprint requests to: D.V. Beloplotov, Institute of High Current Electronics, Russian Academy of Science, Akademicheskoy Avenue 2/3, Tomsk, 634055, Russia. E-mail: rff.qep.bdim@gmail.com

RE beam current even using modern oscilloscopes. The duration and amplitude of the RE beam current depend on the designs of the gas-filled diode and cathode, the amplitude and rise time of the voltage pulse, as well as the kind and pressure of a gas. For example, the parameters of the RE beam under non-optimal conditions can vary from pulse to pulse by more than an order of magnitude due to instability of the amplitude and rise time of the voltage pulses applied across the gas-filled diode. In addition, the RE beam parameters registered behind an anode foil can also be unstable even for the same parameters of the voltage pulses as a result of changes in the state of the cathode surface that occur in atmospheric-pressure air and nitrogen in each pulse due to the formation of cathode spots. Second, registration systems with an insufficient time resolution were used in the experiments performed before 2005. Therefore, it was impossible to measure the electric characteristics of the discharge with a subnanosecond time resolution and directly measure of the parameters of the RE beam. To correctly measure the electric characteristics of the discharge, it is necessary to use voltage dividers, low-inductance shunts, collectors, connectors, cables, attenuators, and oscilloscopes with a sufficiently wide (>6 GHz) transmission band. Third, the measured parameters can substantially depend on the measurement methods. As a consequence, the results obtained in different research groups may differ considerably even when using similar devices. For example, in (Babich, 2003; Babich & Loiko, 2010, 2015; Tarasova *et al.*, 1974), where a non-optimal design of the gas-filled diode and cathode were used, the numbers of electrons in the RE beam was found to be $(6-9) \times 10^8$, while in (Kostyrya *et al.*, 2010, 2012) – $(5-6.2) \times 10^{10}$. There is no consensus on the RE energy distribution. It was asserted in (Babich, 2003; Babich & Loiko, 2015) that, the RE energy distribution reaches its peak value at an energy of 290 keV for a gap with length of 2 cm and amplitude of voltage $U_m = 190$ kV. Moreover, according (Babich, 2003; Babich & Loiko, 2015) a monoenergetic RE beam with electron energies exceeding eU_m (where U_m is the amplitude of the gap voltage and e is the electron charge) is mainly generated in atmospheric-pressure air. Note also that, in (Babich & Loiko, 2010), the results obtained by the same authors were changed. The peak in the RE energy distribution was downshifted to 270 keV, while the gap voltage was increased to 270 keV.

In our works (Tarasenko *et al.*, 2008c; Baksht *et al.*, 2010; Tarasenko, 2011; Kozyrev *et al.*, 2015), it was shown that at applying voltage pulses from the SLEP-150, SLEP-150M, and RADAN-220 pulsers across a gap filled with atmospheric-pressure air the energy spectrum of REs downstream an anode foil consists of two to three groups of electrons with different energies. The main group of electrons have energy lower than eU_m (usually, by a few tens of keV), while the number of electrons with energies higher than eU_m does not exceed 10% of the total number of REs (for the case of a spherical cathode). In addition, there are a

large number of electrons with energies from several units to several tens of keV. On the basis of RE beam absorption curves in foils, the authors of (Mesyats *et al.*, 2012) asserted that the maximum RE energy does not exceed eU_m .

In this paper, detailed experimental studies of the amplitude–temporal characteristics of the discharge and RE beams generated during subnanosecond breakdown in atmospheric-pressure gases with the highest possible resolution time and determine the time at which REs appear behind the anode foil was performed. Here we also compare the main results obtained by the research groups that contributed most to the experimental studies of the generation of RE beams in atmospheric-pressure air. It is rather actual, because the earlier mistakes are often repeated in new works; see, for example Babich & Loiko, (2015), where erroneous data on the RE spectrum were given. It was reported by the authors of (Babich & Loiko, 2015) that they studied picosecond pulses, although their diagnostic equipment did allow them to record pulses even with a duration of 100 ps. We propose to refer to RE pulses with a full-width at half-maximum (FWHM) of 1–50 ps as picosecond ones, while to those with an FWHM of 50–500 ps as subnanosecond ones.

2. EXPERIMENTAL SETUP AND MEASUREMENT METHODS

The parameters of RE beam generated during subnanosecond breakdowns in air, nitrogen, and other gases were studied using experimental setups consisting of the SLEP-150 (Kostyrya *et al.*, 2010; Tarasenko, 2011), SLEP-150M (Tarasenko *et al.*, 2008a; Tarasenko, 2011; Kostyrya *et al.*, 2012), and RADAN-220 pulsers (Zagulov *et al.*, 1989); discharge chambers, and a registration system. Figure 1 shows the design of the output of the RADAN-220 pulser with a gas-filled diode, shunt, and collector.

A negative voltage pulses produced by the pulser was applied via short transmission line (1) to electrode (4) with a

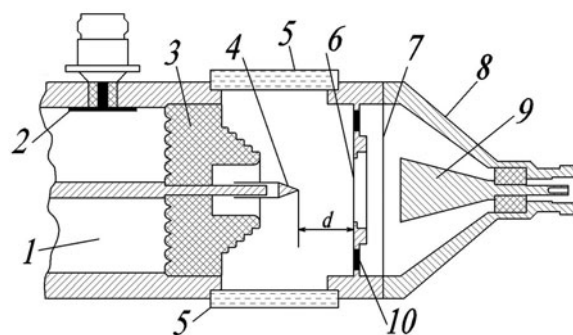


Fig. 1. Schematic representation of the output of the RADAN-220 pulser with the gas-filled diode, shunt, and collector: 1 – transmission line, 2 – capacitive voltage divider, 3 – insulator, 4 – conical cathode, 5 – quartz windows, 6 – foil or grid anode, 7 – Al foil, 8 – collector case, 9 – 20-mm-diameter receiving part of the collector, and 10 – film low-inductance chip resistors.

small curvature radius. The voltage was registered with capacitive voltage divider (2), located upstream of the discharge gap. The RADAN-220 pulser formed voltage pulses with an amplitude of about 250 kV in the idle mode. The FWHM of the voltage pulse at a matched load is ~ 2 ns, and the rise time of the voltage pulse in the transmission line is ~ 0.5 ns. The discharge current was registered with current shunt (10) made of film low-inductance chip-resistors. Stainless-steel potential electrode (cathode) (4) had the shape of a cone with a vertex angle of 82° and a base diameter of 6 mm. The radius of the curvature of the cone vertex was ~ 0.1 mm. In some experiments, a 6-mm-diameter tubular electrode made of a 100- μm -thick stainless-steel foil, as well as an electrode made of a sewing needle were used. Flat grid (or foil) grounded electrode (anode) (6) was placed at a distance of 4–16 mm from the edge of potential electrode (4). When using a grid grounded electrode, 10- or 50- μm -thick Al foil (7) was placed in front of the collector in order to suppress the displacement current. On this setup, the RE beam was registered with collector (8) with 20-mm-diameter receiving area (9).

Figure 2 shows the design of the output of the SLEP-150 pulser, the gas-filled diode, and the collector with a 3-mm-diameter receiving area.

One electrode of the high-voltage line of pulser (1) is the case of peaking spark gap (2). This allowed us to decrease the length of the line and form a voltage pulse of an amplitude of about $\cong 150$ kV and FWHM of $\cong 1$ ns at a matched load. The voltage pulse rise time was determined by the peaking spark gap and was $\cong 250$ ps at a level of 0.1–0.9 at the optimal operation of the one. Gas-filled diode (5) was connected to high-voltage line (1) through short transmission line (3) with a wave impedance of 100 Ω . The amplitude

of the voltage pulse in the transmission line depended on the breakdown voltage of peaking spark gap (2) and, with different peaking spark gaps, could vary from 120 to 200 kV. In the idle mode, the voltage amplitude was doubled upon the arrival of the voltage pulse to the gas-filled diode. In this device, different types of cathodes were used: 6-, 7-, and 20-mm-diameter tubular cathodes made of a 100- μm -thick stainless-steel foil, conical cathodes with a vertex angle of 82° and a base diameter of 6 mm, needles, and a sphere with a diameter of 9.5 mm. A 3-mm-high ring with a 30- or 40-mm-diameter bottom on the edge of which 0.2-mm-diameter wires were stretched parallel to one another with a step of 4 mm was also used as a grid cathode. The distance from the wires to the bottom of the grid cathode was 1.5 mm. The design of such a cathode with a diameter of 40 mm was described in detail in (Kostyrya *et al.*, 2012). The anode of the gas-filled diode was made of 10- μm -thick aluminum foil (8), which was reinforced with grid or collimator (9) from the side of the collector. In some experiments, the foil was replaced with a grid with a transparency of 14, 18, or 64% for a light. The RE beam current (the number of electrons) was registered using collectors with 3- and 20-mm-diameter receiving areas. The total number of electrons in the RE beam behind the foil was measured using a 56-mm-diameter collector. The time resolutions of the collectors with the 3- and 20-mm-diameter receiving areas reached 20 and 80 ps, respectively. Capacitive voltage divider (4) was placed in the output of the pulser, which was filled with transformer oil. The distance from the capacitive divider to the end of the gas-filled diode, to which the foil or grid was fixed, was 22 mm. The gap length d could be varied from 0 (shortcut circuit) to 34 mm.

Some experiments were performed with the SLEP-150M pulser, which had an additional transmission line with built-in capacitive voltage dividers. In this case, it was possible to register both the incident (propagating from the pulser) voltage pulse and that reflected from the gas-filled diode. This allowed us to reconstruct the gap voltage with a higher accuracy than in measurements with capacitive divider (4) (Fig. 2). In some experiments with the SLEP-150M pulser, a transmission line with an air-filled cutting spark gap was used (Tarasenko *et al.*, 2009). This made it possible to form voltage pulses with FWHMs of 0.1 and 0.2 ns. The gas-filled diodes were usually filled with atmospheric-pressure air. We also performed experiments with other gases: nitrogen, helium, neon, argon, krypton, xenon, CH_4 , and SF_6 .

Signals from the capacitive voltage divider, current shunt, and the collector were recorded using LeCroy WaveMaster 830Zi-A (30 GHz, sampling time of 12.5 ps) and Tektronix DSA72504D (30 GHz, sampling time of 10 ps) digital oscilloscopes. The signals were transferred to the oscilloscope through 1-m-long RG58-A/U (Radiolab) high-frequency cables with Suhner 11 N-50-3-28/133 NE and SMA (Radiall R125.075.000) connectors. To attenuate the signals, 142-NM (Barth Electronics) high-frequency attenuators with a transmission band of up to 30 GHz were applied. At registration

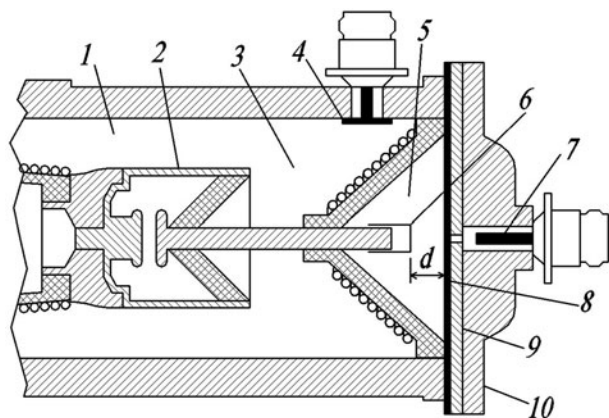


Fig. 2. Schematic of the output of the SLEP-150 pulser, gas-filled diode, and collector with the 3-mm-diameter receiving area: 1 – high-voltage line of the pulser, 2 – peaking spark gap, 3 – transmission line, 4 – capacitive voltage divider, 5 – gas-filled diode, 6 – tubular cathode, 7 – receiver part of the collector, 8 – foil, 9 – 5-mm-thick collimator with a 1-mm-diameter hole, and 10 – collector case. On the left, several turns of the high-voltage coil of the pulsed transformer are shown. On the right, the inductance coil connecting the inner electrode of the transmission line to the pulser case is shown on the insulator.

RE beam by the collector with the 3-mm-diameter receiving area, the electric signal from it was transmitted to the oscilloscopes without attenuators. The oscilloscopes were triggered by the signal from the capacitive voltage divider. The voltage pulses, discharge current, and RE beam current were registered simultaneously per one pulse. The RE beam and X-ray emission were also registered with an RF-3 film enveloped in 120- μm -thick black paper. The discharge plasma glow was photographed using a Sony A100 digital camera.

It was proposed in (Tarasenko *et al.*, 2003a) to call the RE beam registered behind the foil anode a supershort avalanche electron beam (SAEB). Below we will use this term. The use of the term SAEB is substantiated in (Baksht *et al.*, 2014). Note that the pulsers, collectors, and measurement methods of SAEB current and voltage pulses applied across the gas-filled diode were described in detail in our previous works (Tarasenko *et al.*, 2008a, 2008c, 2009, 2013b; Baksht *et al.*, 2010, 2014; Kostyrya *et al.*, 2010, 2012; Tarasenko, 2011, 2014; Rybka *et al.*, 2012; Shao *et al.*, 2013; Beloplotov *et al.*, 2014a; Kozyrev *et al.*, 2015), as well as in (Mesyats *et al.*, 2012, 2013; Sharypov *et al.*, 2014), while no schemes of the magnetic spectrometer, the transition unit between the gas-filled diode and magnetic spectrometer, the Faraday cup, the shunt, and other important components substantially affecting the measured parameters were given in (Babich, 2003; Babich & Loiko, 2010, 2015) and other publications of that research group.

3. EXPERIMENTAL RESULTS AND DISCUSSION

3.1. Observed Forms of Discharge in Atmospheric-Pressure Air and Nitrogen

The form of the discharge excited after applying a nanosecond voltage pulse to a gap with a non-uniform distribution of the electric field depends on the gap length d (Tarasova *et al.*, 1974; Babich, 2003; Yakovlenko, 2007; Tarasenko *et al.*, 2008a; Levko *et al.*, 2012; Tarasenko, 2014). At large values of d , a diffuse corona discharge forms near the

cathode. As d decreases, the diffuse discharge fills the entire gap and the brightness of its glow increases. In (Tarasenko *et al.*, 2003a), this discharge mode was proposed to be called a volume discharge initiated by an avalanche electron beam (VDIAEB). In the English-language papers, we use more short term REP DD – Runaway Electrons Preionized Diffuse Discharges. The REP DD was discussed in detail in (Tarasenko, 2014). Figure 3a and 3b shows photographs of the plasma glow of REP DDs in nitrogen and air obtained on the setup with the RADAN-220 pulser (see Fig. 1).

An atmospheric-pressure diffuse discharge forms in both nitrogen and air. Bright spots appear only on the cathode with a small curvature radius. Short anode-directed spark leaders growing from the cathode spots are also seen. In the gas-filled diode filled with nitrogen, the diffuse discharge is visually more uniform and contacts the side surface of the tubular cathode (Fig. 3a). It is seen in the photograph of the REP DD in air that the diffuse discharge consists of separate jets (Fig. 3b).

Figure 3c shows a photograph of the integral REP DD plasma glow taken from the side of the grid anode on the setup with the SLEP-150 pulser. A bright glow consisting of diffuse jets, which are closed on the grid, is observed near the annular cathode. At observation of the REP DD plasma glow in atmospheric-pressure nitrogen or air through the side window (Fig. 3a, 3b), the glows of separate jets in the integral photographs overlap and, they become almost indistinguishable. As the gas pressure increases, the diameters of separate diffuse jets decrease and they become visible when being observed through the side window (Tarasenko, 2014). At pressures below the atmospheric one, the diffuse jets overlap and they are usually not seen in the integral photographs. Bright spots from which diffuse jets emerge are seen at the cathode edge (Fig. 3c) as in Figure 3a and 3b. Short small-diameter diffuse jets that do not reach the grid are also observed. In Figure 3c, a low-intensity air glow is also observed in the region of the gas-filled diode remote from the cathode. It is seen from Figure 3c that the axial region of the gap with diameter nearly equal to the diameter of

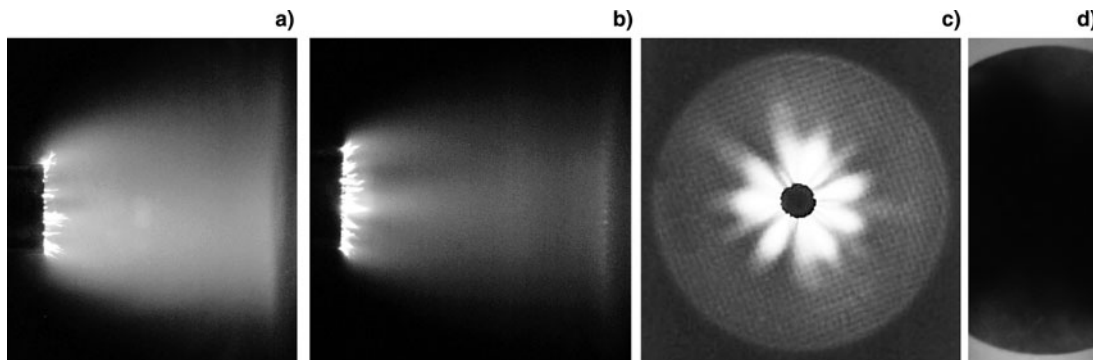


Fig. 3. Time-integrated images of the discharge plasma glow in atmospheric-pressure nitrogen (a) and air (b, c), as well as SAEB print on an RF-3 film (d), obtained on the setups with the RADAN-220 pulser (a, b) and the SLEP-150 pulser (c, d) per one pulse. Gap lengths is 14 mm (a, b) and 11 mm (c, d). The diameter of the tubular cathode located on the left in frames (a) and (b) is 6 mm, and that of the tubular cathode located in the centers of frames (c) and (d) is 7 mm.

the tubular cathode has the lowest glow intensity. However, at $d = 12$ mm, no decrease in the blackening of the RF-3 film near the axis of the gas-filled diode with the 6-mm-diameter tubular cathode was observed in the print of the RE beam (Fig. 3d). The difference between the regions of the REP DD plasma glow and the print of the electron beam is due to the fact that the SAEB is generated about 300 ps after applying the voltage pulse to the gap and has a duration of about 100 ps, whereas the plasma glow lasts for several tens of nanoseconds and reaches its maximum intensity about 500 ps after SAEB generation (Tarasenko et al., 2008a; Levko et al., 2012; Tarasenko, 2014). In addition, the SAEB electrons are emitted into a wide angle, due to which the size of the beam print increases substantially (Tarasenko et al., 2008a). As the diameter of the tubular cathode increases, both the film blackening and the SAEB current density near the diode axis decrease (Tarasenko, 2011).

At $d \leq 10$ mm, a cathode-directed spark leader formed on the background of the diffuse discharge on the setups with the SLEP-150, SLEP-150M, and RADAN-220 generators. As the gap length decreased, the spark leader transformed into a spark channel (Lomaev et al., 2009; Shao et al., 2012; Tarasenko et al., 2013b; Beloplotov et al., 2014b). As d decreased further, the brightness of the spark channel increased and the diffuse discharge became almost invisible. However, our studies have shown that, at a nanosecond rise time of the high-voltage pulse, the discharge in a gap with a non-uniform electric field first operates in the diffuse mode and, then, constricts (Lomaev et al., 2009; Shao et al., 2012; Tarasenko et al., 2013b; Beloplotov et al., 2014b; Tarasenko, 2014). As will be shown below, the SAEB is generated in the initial stage of the discharge, thereby providing REP DD formation.

3.2. Waveforms of the Voltage and Discharge Current Pulses

Figure 4 shows waveforms of the voltage pulses and the current through the gap for three values of d . When the REP DD forms on the setups with the RADAN-220 and SLEP-150 pulsers, the resistance of the diffuse discharge plasma is usually lower than the wave impedance of the pulsers. As a result, an oscillatory discharge mode takes place. At $d = 12$ and 18 mm, no more than five half-periods are observed in the waveform of the discharge current (Fig. 4b). As the gas pressure and/or the gap length d increase, as well as when the gas-filled diode is filled with electronegative gas SF₆, the resistance of the discharge plasma increases and an aperiodic discharge mode takes place.

At $d = 6$ mm (Fig. 4), the amplitude of the gap voltage, as was expected, decreased and both the amplitude of the discharge current and the number of current half-periods increased. The results obtained using an HSFC PRO high-speed four-channel CCD camera with the minimal exposure of 3 ns (Shao et al., 2012; Tarasenko et al., 2013b) show

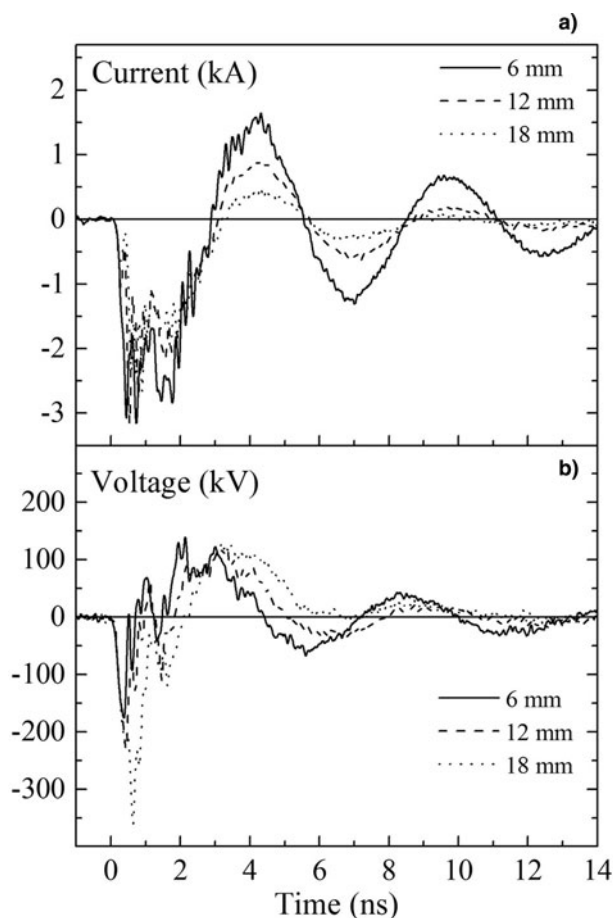


Fig. 4. Waveforms of the voltage (a) and discharge current (b) pulses at different gap lengths. The cathode is a 6-mm-diameter tube. The waveforms were obtained on the setup with the SLEP-150 pulser.

that, at small values of d , the gap is bridged by the spark channel in several nanoseconds or less. This leads to an even larger decrease in the plasma resistance in the discharge gap and an increase in the number of oscillations of the discharge current. However, under these conditions, even at small d , the SAEB is observed in the beginning of the diffuse discharge stage before the formation of the spark channel.

Figure 5 demonstrates the initial segments of the voltage and current waveforms shown in Figure 4.

In these waveforms, obtained with a high time resolution, one can distinguish three typical discharge stages that were described for the first time in our works (Tarasenko et al., 2008a, b, c). When the voltage pulse is applied to the gap, the well-known displacement current of a “cold” diode, that equal $C(dU/dt)$ (where C is the capacitance of the “cold” diode and U is the gap voltage), is first registered (time interval A in Fig. 5). By the “cold” diode we mean a diode in which there is still no dense plasma that “pushes out” the electric field. Note that Figure 5 shows the voltage pulses detected by the capacitive divider located at a distance of 22 mm from the anode of the SLEP-150 pulser. First, the

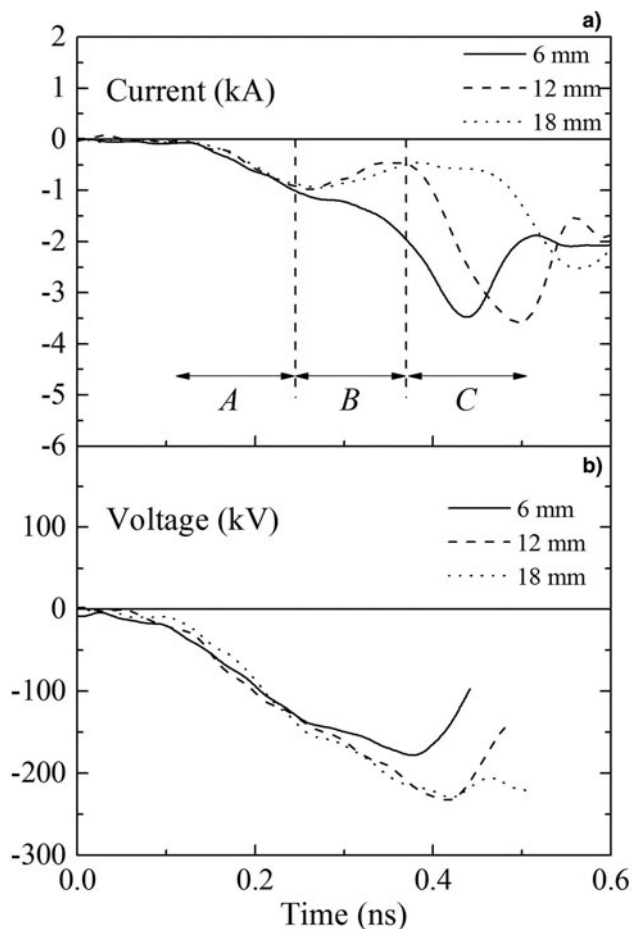


Fig. 5. Waveforms of the voltage (a) and discharge current (b) pulses registered in the initial stage of the discharge on the setup with the SLEP-150 pulser at different gap length. The cathode is a 6-mm-diameter tube. Time intervals A, B, and C correspond to the current of the “cold” diode (displacement current), dynamic displacement current, and conduction current, respectively.

divider detects the front of the incident wave. About 100 ps later, the front of the reflected wave reaches the divider, after which the divider detects the sum of these two waves. As a result, the waveform of the discharge current pulse in Figure 5 is shifted with respect to the front of the voltage pulse by about 100 ps. At $d = 6$ mm, the displacement current continues to increase $\cong 250$ ps after the voltage pulse has arrived at the capacitive divider, while dU/dt begins to decrease. The decrease in the dU/dt can be seen on the waveforms of the discharge current at $d > 10$ mm. At $d = 12$ and 18 mm, the decrease in the displacement current is observed $\cong 250$ ps after the arrival of the voltage pulse at the capacitive divider, while at $d = 6$ mm, the current through the gap continues to increase. Within time interval B (Fig. 5b), the current through the gap (curve 1) slightly decreases and then increases. This is due to the contribution of the dynamic displacement current $U(dC^*/dt)$, caused by the charging of “compressing capacitor” C^* , formed by the edge of the

dense plasma crossing the gap and the flat anode (Tarasenko *et al.*, 2010a, b, 2015). As was shown in (Tarasenko *et al.*, 2015), after the edge of the dense plasma reaches the anode, the second ionization wave with a higher velocity passes through the gap in the opposite direction. In this case, the current through the gap is determined by the conduction current (time interval C in Fig. 5b). At $d = 12$ and 18 mm, the discharge current (Fig. 5b; curves 2, 3) reaches its peak value later than at $d = 6$ mm (Fig. 5b, curve 1). The time delays are about 50 and 100 ps, respectively. This is because, at larger values of d , a longer time is required for the ionization wave to traverse the gap.

Thus, the time evolution of the discharge current in the REP DD includes three stages: the displacement current of the “cold” diode, the dynamic displacement current, and the conduction current. As will be shown below, the SAEB is generated mainly in the stage of the dynamic displacement current. It should also be kept in mind that, within time interval B, the current between the plasma edge and the anode is determined by the dynamic displacement current and the SAEB current, while that between the cathode and the edge of the dense plasma is determined by the conduction current. The current shunt records the sum of the dynamic displacement current and the SAEB current. These currents are difficult to separate, because the amplitude of the dynamic displacement current is, as a rule, much higher. For example, with the grid cathode, the amplitude of the dynamic displacement current reaches 2 kA (Shao *et al.*, 2013).

3.3. Waveforms of the SAEB Current Pulses and Their Shift Relative to Those of the Voltage and Discharge Current Pulses

There are only two research groups in which the waveforms of the SAEB current behind the anode foil were registered with a time resolution of several tens of picoseconds (Kostyr-ya *et al.*, 2012; Mesyats *et al.*, 2012, 2013; Rybka *et al.*, 2012; Sharypov *et al.*, 2014; Tarasenko *et al.*, 2013a, b). However, only in our works (Tarasenko *et al.*, 2008a, b, c; Burachenko & Tarasenko, 2010; Tarasenko, 2011), the waveforms of the SAEB current were synchronized with those of the voltage and discharge current pulses. Than a time resolution of the registration system is ~ 100 ps, it is not difficult to synchronize voltage in the idle mode and discharge current pulses. The displacement current of the “cold” diode and the front of the voltage pulses on the gap are synchronous in time, hence the peak of the displacement current corresponds to the maximum of dU/dt . To provide a more accurate synchronization of the waveforms of the voltage pulses with the ones of the discharge current, it is necessary to reconstruct the voltage on the gap from the waveforms of an incident and reflected voltage pulses. To this end, the SLEP-150M pulser was equipped with an additional transmission line with built-in capacitive voltage dividers allowing one to register the incident and reflected voltage pulses separately.

In these experiments, the waveforms of the SAEB current registered with the collector were synchronized with the waveforms of the voltage pulse on the gap and discharge current in the same way as in (Tarasenko *et al.*, 2008a, b, c; Burachenko & Tarasenko, 2010; Tarasenko, 2011), that is, by means of the displacement current of the “cold” diode. To this end, a grid anode was used, which made it possible to record the displacement current by the collector. Varying the size of the grid cell while keeping its transparency, it was possible to control the amplitude of the displacement current of the “cold” gas-filled diode that are recorded by the collector while keeping the amplitude of the SAEB current unchanged. In this way, it was possible to make the amplitude of the displacement current sufficient for synchronization with the front of the voltage pulse and, thereby, to synchronize the waveforms of the discharge current and the SAEB current pulses with that of the voltage pulse. Note that the effect of the grid cell size on the value of the displacement current was not taken into account in (Babich & Loiko, 2010), which, along with the low resolution of the registration system [in (Babich & Loiko, 2010), a TDS 3052B oscilloscope with a transmission band of 500 MHz was used], led the authors of (Babich & Loiko, 2010) to the erroneous conclusion on the registration of an “electromagnetic” pickup in our works. The dynamic displacement current in (Tarasova & Khudyakova, 1969; Tarasova *et al.*, 1974; Babich, 2003, Babich & Loiko, 2010, 2015) could not be registered because of the insufficient time resolution of the oscilloscope, the Faraday cup, and the shunt made of TVO resistors.

In the present work, as in (Tarasenko *et al.*, 2008a, b, c, 2015; Burachenko & Tarasenko 2010), the amplitude of the dynamic displacement current was comparable with that of the SAEB current registered with the collector when a specially selected grid was used as an anode. To determine the moment of SAEB generation, the signals from the collector behind the foil anode and the grid anode were recorded at the same voltage pulses and/or discharge current pulses. This allowed us to determine the position of the SAEB current pulses with respect to other pulses with an accuracy of several tens of picoseconds. Figure 6 presents an example of synchronization of waveforms of the SAEB current pulses with that of the voltage pulses when using the grid (Fig. 6; curves 1, 3) and foil (Fig. 6; curves 2, 4) anodes.

In Figure 6 (as in Fig. 5), signals from the capacitive voltage divider of the SAEB-150 generator located at a distance of 10 mm from the cathode edge are shown. In this case, the front of the incident voltage wave was registered $\cong 60$ ps earlier. Due to the special choice of the grid transparency and the grid cell size, the amplitudes and trailing edges of the collector signals obtained with the grid and foil anodes are determined by the SAEB current. A large-amplitude positive spike in the waveform of the collector signals (Fig. 6b, curve 3) after the SAEB pulse in the case of the grid anode is associated with the effect of the positive charge of ions, which remain near the anode after REs escape through the

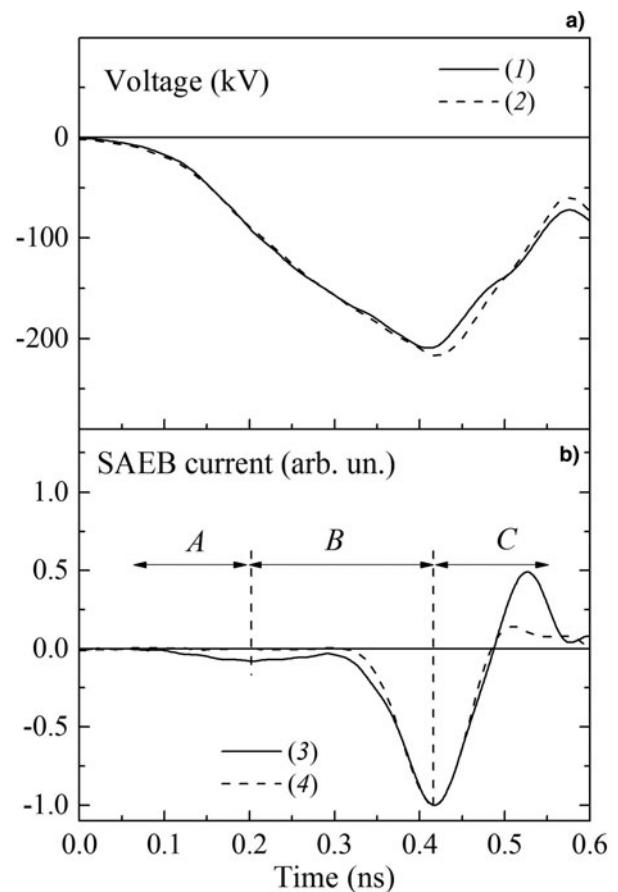


Fig. 6. Waveforms of the voltage (a) and the SAEB current (b) pulses. The SAEB was registered by collector with the 20-mm-diameter receiving area: 1, 3 – the anode is a grid with a transparency of 64%; 2, 4 – the anode is a 10- μm -thick aluminum foil. The cathode is a 6-mm-diameter tube. The gap length is $d = 12$ mm. The waveforms were obtained on the setup with the SLEP-150 pulser. Time intervals A, B, and C correspond to the current of the “cold” diode (displacement current), dynamic displacement current, and conduction current, respectively.

grid. In the case of the grid anode, the initial segment of the collector signal (Fig. 6b, time interval A) is related to the displacement current of the “cold” diode. Then, the collector detects the dynamic capacitive current and the SAEB current (Fig. 6b, time interval B). As in the case of registration of the discharge current with the shunt (Fig. 5a), the dynamic displacement current at a gap length of 6 mm begins to be registered about 250 ps after the arrival of the voltage pulse at the capacitive divider. This means that, by this time, the first electrons have already been emitted from the cathode and the plasma begins to form in the gap and propagate toward the anode. It is assumed that, at gap lengths of 12 and 16 mm, the first REs also appear with a time delay of about 250 ps after the arrival of the voltage pulse at the capacitive divider and 200 ps after the appearance of the displacement current of the “cold” diode. However, as the gap length d increases, the formation rate of the dense plasma near the cathode decreases due to a decrease in the electric field strength with distance from the cathode. As a result,

within time interval B , the current signal from the collector and shunt decreases (see Figs 5 and 6).

At $d = 12$ mm and atmospheric-pressure air, the peak of the SAEB current nearly coincides with the maximum of the voltage pulse (Fig. 6). It should be taken into account that the receiving area of the collector is located at a distance of 5 mm from the anode. Electrons with energies of ≈ 150 keV travel this distance over 30 ps. Thus, electrons in the peak of the SAEB current come from the foil anode only 30 ps earlier. In (Tarasenko *et al.*, 2008b, c), the energy of electrons of the main SAEB group for $d = 12$ mm, a tubular cathode, and the voltage amplitude of ≈ 170 kV was found to be ≈ 150 keV. Under the conditions of Figure 6, the voltage amplitude was ≈ 220 kV, that is, it was lower than that in idle mode (which under these conditions exceeded 350 kV), but higher than in (Tarasenko *et al.*, 2008b, c). The increase in the voltage amplitude leads to an increase in the electron energy and, accordingly, a faster arrival of SAEB electrons at the collector.

Figure 7 shows waveforms of the voltage and SAEB current pulses for different gap lengths d .

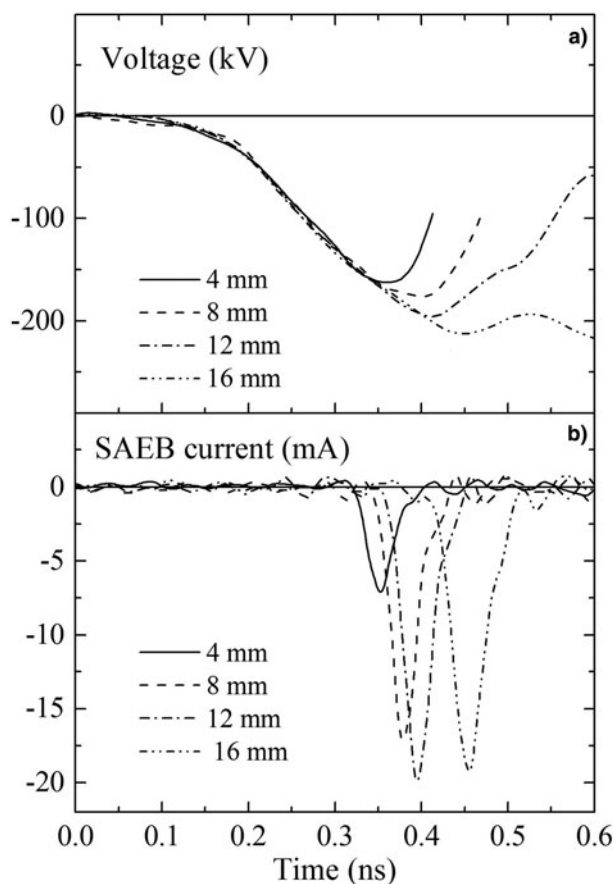


Fig. 7. Waveforms of the voltage (a) and the SAEB current (b) pulses. The SAEB was registered by collector with the 3-mm-diameter receiving area, located behind a 5-mm-thick collimator with a 1-mm-diameter hole and a 10- μ m-thick aluminum foil at different gap length. The cathode is a 6-mm-diameter tube. The waveforms were obtained on the setup with the SLEP-150 pulser.

The collector with the 3-mm-diameter receiving area and a 5-mm-thick collimator with a 1-mm-diameter hole were used during registration of SAEB. As was shown in (Rybka *et al.*, 2012; Tarasenko *et al.*, 2013a, b), this allowed us to correctly register the SAEB current pulse, the FWHM of which was ≥ 25 ps. As d was reduced, the maximum gap voltage decreased and the time delay of the SAEB current pulse registered with the collector behind the foil anode with respect to the front of the voltage pulse reached its minimal value. In these experiments, the synchronization accuracy of different SAEB current pulses to each other as well as the one of different voltage pulses was better than 10 ps. Furthermore, the synchronization accuracy of the SAEB current pulses to the voltage pulses was no worse than several tens of picoseconds.

An increase in the time delay of the SAEB current from the collector with increasing gap length can be associated with a slower formation of the dense plasma near the cathode and a slower passage of the front of the first ionization wave through the discharge gap. In addition, as the gap length increases, a longer time is required for the ionization wave to traverse the gap. Furthermore, the distance between the peaking spark gap and the anode plane was fixed, the gap length was varied by moving the tubular cathode in the gas-filled diode along the cathode holder (the inner conductor of the transmission line, see Fig. 2). As a result, at the large gap length d the incident voltage pulse arrived to the cathode edge earlier than at the small one. The voltage amplitude increases at the gap length increase. The increase in the breakdown voltage indicates that the formation rate of the dense plasma near the cathode and in the gap decreases with increasing gap length. In long gaps, the dynamic displacement current increases slower and a maximum is observed in the waveform of the displacement current of the “cold” diode (Figs 5 and 6). Under these conditions, the ionization wave bridges the discharge gap over a longer time. Accordingly, the voltage begins to decay later and the SAEB duration somewhat increases. In Figure 7, the duration of the SAEB current pulse is the highest at $d = 16$ mm. It is seen from Figure 7 that, for the 6-mm-diameter tubular cathode, a 12-mm-long gap is optimal for obtaining the largest SAEB amplitude. Measurements performed with the collector with a 20-mm-diameter receiving area also show that the SAEB currents is maximum at $d = 12$ mm. An increase in the length of the sharp cathode edge (using of a grid cathode, an increase in the diameter of the tubular cathode) leads to a decrease in both the optimal gap length and the gap voltage. It is of interest to examine how the SAEB parameters depend on the propagation time of the voltage wave with a rise time of ~ 300 ps over the working surface of the grid cathode, with which the largest number of SAEB electrons was obtained (Kostyrya *et al.*, 2012). Figure 8 shows waveforms of the SAEB current pulses passed through a 1-mm-diameter hole of the collimator that was located on the axis of the gas-filled diode or displaced from the axis by 19 mm in the radial direction. A 30-mm-diameter grid cathode was used.

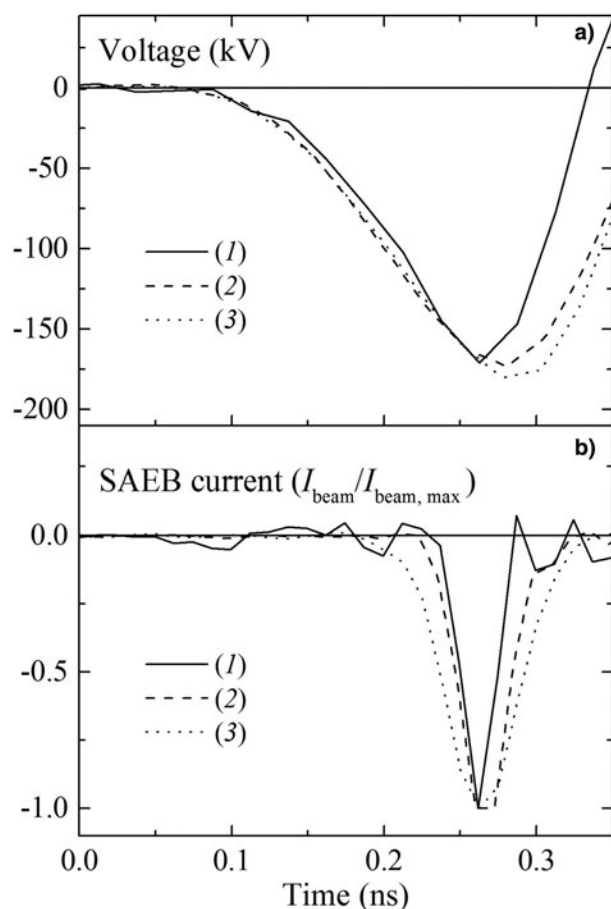


Fig. 8. Waveforms of the voltage (a) and the SAEB current (b) pulses. The SAEB was registered by a collector with the 3-mm-diameter receiving area, located behind a collimator with a 1-mm-diameter hole and a 10- μ m-thick aluminum foil: 1 – per one pulse; 2, 3 – averaged over 25 pulses. The collimator hole is located on the axis of the gas-filled diode (1, 3), and at a distance of 19 mm from the axis (2). The gap length is 6 mm. The cathode is a grid fixed on a 30-mm-diameter ring. The waveforms were obtained on the setup with the SLEP-150 pulser.

Waveform 1, obtained per one shot, demonstrates the time resolution of the registration system. Among 50 waveforms, this is the waveform with the minimal (under these conditions) SAEB duration. Waveforms 2 and 3 are averaged over 25 pulses. Comparison of waveforms 1, 2, and 3 shows that the electron beams from center of the cathode (waveform 3) and from a peripheral area (waveform 2) are generated simultaneously (to within 20 ps). The generation of SAEB is more stable in the peripheral areas of the cathode. In waveform 2, the FWHM of the SAEB current pulse is smaller than in waveform 3 and is close to that in waveform 1, registered per one pulse.

3.4. Effect of the Collector, Collimator, and Cathode on the Amplitude and Duration of the SAEB Current

Direct detection of an SAEB pulse with an FWHM of ~ 100 ps, which corresponded to the actual SAEB duration,

was reported for the first time in (Tarasenko *et al.*, 2005). The SAEB duration was measured using a collector with a time resolution of ~ 50 ps and corresponded to the limiting time resolution of the TDS-6604 oscilloscope (6 GHz, sampling time of 50 ps) used in (Tarasenko *et al.*, 2005). To resolve the leading and trailing edges of the SAEB current pulse, it is necessary to have at least three sampling points within them. For the sampling time of 50 ps, the minimal resolvable durations of the leading and trailing edges of the pulse are 100 ps. For a triangular SAEB pulse, this corresponds to the 100-ps-long FWHM. As was shown later in (Tarasenko, 2011; Kostyrya *et al.*, 2012), this duration was nearly equal to the durations of SAEB pulses registered behind the gas-filled diode foil under similar conditions. Figure 9 shows waveforms of SAEB current pulses obtained with different collectors and cathodes and different collimators.

The SAEB current pulse shown in Figure 9a was registered by the collector with the 3-mm-diameter receiving area behind a 5-mm-thick collimator with a 1-mm-diameter hole. For a spherical cathode and a gap length of 6 mm, the FWHM of the SAEB was $\cong 25$ ps. The minimal durations of the SAEB current pulses were achieved with spherical and conic cathodes for gap lengths as short as 2–6 mm. The SAEB duration increases with increasing gap length and when using a tubular cathode with the length of the emitting edge of 19 mm. The FWHM of the SAEB current pulse shown in Figure 9b is $\cong 40$ ps. The duration of the SAEB pulse became even longer when the diameter of the collimator hole increased, while the collimator thickness decreased (Fig. 9c–9e). The FWHM of the SAEB pulse was $\cong 45$ ps when using a 250- μ m-thick copper collimator with a 4-mm-diameter hole (Fig. 9c).

The SAEB current pulse with the FWHM of $\cong 80$ ps shown in Figure 9d demonstrates the resolution capability of the collector with a 20-mm-diameter receiving area. The pulse registered from a considerable part of the anode foil by the collector behind a copper collimator with an 18-mm-diameter hole (Fig. 9e) has a typical SAEB pulse duration of ~ 100 ps. SAEB pulses with similar durations were also registered when using cathodes of different design, as well as in discharges in atmospheric-pressure nitrogen and other gases. This unambiguously indicates that the duration of SAEB pulses behind the anode foil of a gas-filled diode is ~ 100 ps, rather than less than 50 ps, as was stated in (Mesyats *et al.*, 2008; Babich & Loiko, 2015). For the first time, a decrease in the SAEB duration with decreasing collector dimensions was observed in (Tarasenko *et al.*, 2003b). As the thickness of the anode foil increased, the duration of the SAEB pulse changed insignificantly when using collectors with both 3- and 20-mm-diameter receiving areas.

Note that, under certain conditions, a decrease in the parameter U/pd (where p is the gas pressure) (Baksh *et al.*, 2007, 2008a; Tarasenko *et al.*, 2012a) or the screening of the sharp cathode edge lead to the generation of an SAEB consisting of two pulses (Mesyats *et al.*, 2013). The time

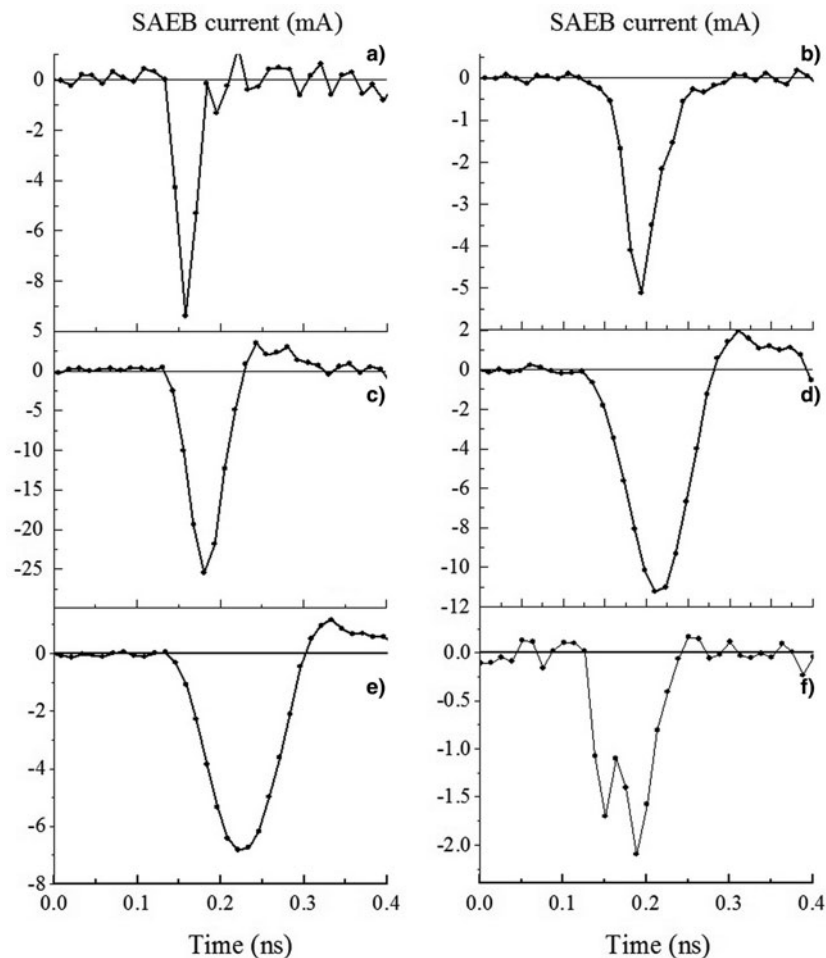


Fig. 9. Waveforms of the SAEB current pulses registered by a collector with diameter receiving area of 3 (a–c, f) and 20 mm (d, e). The collector was located behind a collimator with a hole diameter of 1 (a, b, f), 4 (c), and 18 mm (d, e). The cathode is a sphere (a) and a tube (b–f). The gap length is 6 (a) and 12 mm (b–f).

interval between the maxima of these pulses exceeded 100 ps, due to which they could be registered using the collector with the 20-mm-diameter receiving area. The formation of two pulses can be explained by a relatively small ($\sim 20\%$) decay of the gap voltage during the generation of the first pulse and the passage of the second ionization wave from the cathode (Baksht *et al.*, 2007, 2008a) during the secondary voltage decay. It is assumed that the second pulse is generated due to electron emission from the front of the second ionization wave, which propagates from the cathode. Due to a decrease in the gap voltage, the electron energy in the second pulse is lower than in the first one and the FWHM of the second pulse is larger. When an SAEB consisting of two pulses is generated, its amplitude decreases.

As was noted in the Introduction, the parameters (amplitude and duration) of the SAEB current can vary from pulse to pulse. The strongest variations are observed under non-optimal conditions and also when using a freshly manufactured cathode. Therefore, before experiments, the cathode was trained over several tens of pulses. Note that, here, for

illustration, we present SAEB pulses obtained at identical voltage pulses and, when using a collimator with a 1-mm-diameter aperture, SAEB pulses of the same shape. In our previous works (Rybka *et al.*, 2012; Tarasenko *et al.*, 2012a, 2012b; Levko *et al.*, 2013; Balzovsky *et al.*, 2015), SAEB pulses having two to three peaks with a time interval between peaks of ~ 30 ps were recorded with a picosecond time resolution. The reliability of registration of the SAEB pulses with an FWHM of ~ 25 ps as well as the picosecond resolution of the registration system consisted of the collector, cables, and connectors are confirmed by measurements of amplitude, phase, and frequency characteristics of the one by using an Agilent Technologies E8363B vector network analyzer in the frequency range of 0.01–40 GHz (Balzovsky *et al.*, 2015). An example of a double-peak SAEB pulse is given in Figure 9f. Such waveforms were most often registered with a tubular cathode at gap lengths shorter and longer than the optimal one. Double-peak pulses were also registered behind thick foils. We consider that two and more peaks are generated due to picosecond time delays between the formation of separate diffuse jets near the cathode and

their subsequent propagation (see Fig. 3c). Since the gap voltage in this case changes insignificantly, double-peak pulses are registered behind thick foils. As the collimator hole diameter increases, the RE fluxes from separate jets are mixed and the double-peak structure of the SAEB current becomes unobservable. Furthermore, due to mixing of electrons from separate jets and an insufficient time resolution, the double-peak structure is difficult to register by the collector with the 20-mm-diameter receiving area even with the use of a collimator.

The largest SAEB current amplitudes in atmospheric-pressure air were recently obtained with the SLEP-150 pulser at an amplitude of the incident voltage wave of 200 kV and a cathode made of wires stretched in parallel on a 40-mm-diameter ring (Kostyrya et al., 2012). The number of electrons in the beam reached 6.2×10^{10} , which corresponds to the SAEB current amplitude of 100 A at an FWHM of ~ 100 ps. In those experiments, a gas-filled diode similar to that shown in Figure 2 was used. Specific features of this diode are that it has the minimal inductance of the junction between the transmission line and the diode and that the entire side surface of the gas-filled diode is covered with an insulator. When the side surface of the gas-filled diode is partially open, the SAEB amplitude decreases. This is achieved by decreasing the insulator length or applying a gas-filled diode the side surface of which is not covered with an insulator (Fig. 1). The decrease in the SAEB current amplitude can be caused by the escape of a substantial fraction of REs onto the open part of the side surface of the gas-filled diode. The application of an internal conical insulator (Fig. 2) results in the arrival of REs generated in the lateral direction (Tarasenko et al., 2008a, b) at its inner wall and the charging of its surface. Apparently, this additional electric field of the negative surface charge of the insulator increases the number of REs arriving at the anode. At a voltage pulse rise time of 1 ns and shorter, the SAEB amplitude depends on the cathode material (Zhang et al., 2013). On the setup with the SLEP-150 M generator, it is shown that the amplitude of the voltage across the gap during the generation of the SAEB depends on the cathode material and reaches the highest value with a stainless steel cathode. When all other factors are equal, the highest maximal amplitudes of the SAEB current are attained with cathodes that ensure the existence of the maximal voltages across the gap.

3.5. Energy of SAEB Electrons

The RE energy spectra were previously studied in our works (Tarasenko et al., 2008c, b; Baksht et al., 2010; Kozyrev et al., 2015). Those studies, as well as results obtained with a high time resolution (Tarasenko et al., 2013a), unambiguously indicate the presence of two to three groups of electrons with different energies in SAEB generated under conditions close to the optimal ones. The energy distribution of the main (the second according to our classification) group of electrons usually has a maximum at an energy that is lower

by several tens of keV than eU_m . Note that, in most experiments with a subnanosecond rise time of the voltage pulse, electrons of the main group are mainly registered. The electrons of the first group have relatively low energies, as a rule, a few tens of keV and less. To register the electrons of this group, one should use thin ($\leq 20 \mu\text{m}$) aluminum anode foils. In our experiments with the SLEP-150M pulser (Tarasenko et al., 2008a, b) and the RADAN-220 generator (Tarasenko et al., 2005), a considerable increase in the SAEB current amplitude was observed with decreasing foil thickness. An example of such a dependence is presented in Figure 10, which along with the experimental absorption curve, shows the calculated attenuations of monoenergetic electron beams in aluminum foils of different thicknesses.

The calculations were performed by the formula taken from (Tabata & Ito, 1975). The experimental curve has two characteristic bends at energies of 30 and 140 keV, which confirm the presence of three groups of electrons with different energies. The electrons of the third group have energies higher than eU_m . However, these electrons are small in number. In experiments with a spherical cathode (which, among all cathodes under study, was optimal for the generation of electrons with energies higher than eU_m), the number of such electrons was no more 10% of the total number of SAEB electrons. This result is confirmed by experiments with the use of a time-of-flight spectrometer (Tarasenko et al., 2008c). Note that, with the use of a spherical cathode, the breakdown gap voltage increased and varied substantially from pulse to pulse.

Experiments with different gap lengths and anode foils of different thickness have shown that, as the gap length (and, accordingly, the gap voltage) increases, the fraction of electrons with elevated energies in the main group increases. However, the number of these electrons is less than the

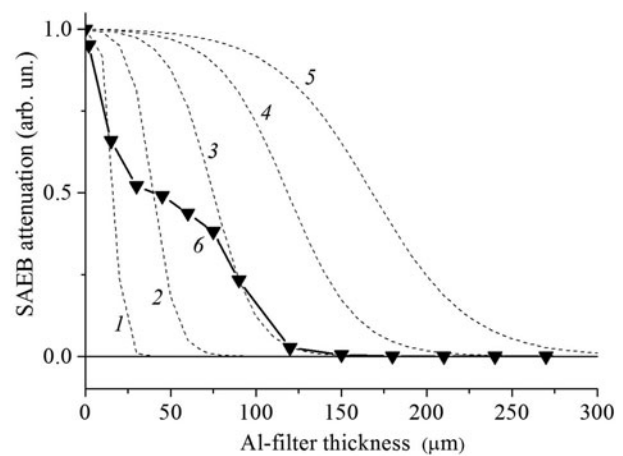


Fig. 10. Calculated numbers of electrons behind aluminum foils of different thickness for monoenergetic beams with different electron energies and experimental SAEB attenuation curve obtained for $d = 12$ mm on the setup with the SLEP-150M pulser with the tubular cathode at $U_m = 170$ kV: 1–50, 2–100, 3–150, 4–200, and 5–250 keV.

number of electrons in the SAEB at the optimal gap length. For example, it follows from the dependence of the number of electrons in the beam on the gap length d that, for the SAEB-150 pulser with a 20-mm-diameter tubular cathode and a 15- μm -thick Al foil anode, the optimal value of d is 6 mm. For a 20- μm -thick Cu foil anode under the same conditions, the largest number of REs was obtained at $d = 14$ mm. Due to an increase in electron energy losses in the anode, it is necessary to rise the gap voltage in order to increase the SAEB current amplitude behind the foil. This was achieved by increasing d without varying the pulser voltage pulse. Similar results were also obtained with the RADAN-220 pulser with the 6-mm-diameter tubular cathode. So, for example, as the anode Al foil thickness increased from 10 to 100 μm , the SAEB current amplitude decreased 24-fold at $d = 8$ mm, sixfold at $d = 12$ mm, and only 2.8-fold at $d = 16$ mm, that is, the fraction of electrons with elevated energies increased with increasing gap length. It is seen from Figure 7 that the breakdown voltage under these conditions increases.

3.6. REs and X-rays downstream of anode foil at pressure more than 0.1 MPa

Until our earliest studies (Alekseev *et al.*, 2003, 2005; Tarasenko *et al.*, 2003a, b; Kostyrya & Tarasenko, 2004), only one scientific group managed to detect a RE beam downstream of an anode foil in atmospheric-pressure air using a Faraday cup (Tarasova *et al.*, 1974; Babich, 2003). By now we are aware of two more groups who succeeded in this using a collector (Mesyats *et al.*, 2006, 2011; Yalandin *et al.*, 2010; Zhang *et al.*, 2015). Noteworthy is also a study that reports on detection of a RE beam and X rays at a N_2 pressure of tens of atmospheres with a special lumino-phore (Ivanov, 2013). Presented below are data of detailed research in the effect of pressure and gas kind on amplitude-time and spatial characteristics of discharges and on SAEB amplitudes in a subnanosecond breakdown of different gases. Note that the time resolution of a collector with which we measured SAEBs downstream of anode foils was ≈ 80 ps (Balzovsky *et al.*, 2015). It is shown that the generation of REs and X rays at negative voltage polarity is a common phenomenon in gas-filled diodes under pressure above 0.1 MPa. Figure 11 presents pressure dependences of the beam current for six gases in an interelectrode gap of 14 mm at a voltage rise time of ≈ 1 ns.

The SAEB was registered downstream of an AlBe foil 45 μm thick and grid with 14% transparency. The voltage pulses produced by the RADAN-220 pulser were applied to the gas-filled diode at increased inductance, and this increased the voltage rise time to ≈ 1 ns, decreased the SAEB current amplitude, and narrowed the range of pressures at which a SAEB was detectable by the collector. However, even with the voltage rise time equal to ≈ 1 ns, we managed to register a SAEB in different gases, including heavy Kr, at a pressure of 0.15 MPa. As the voltage rise

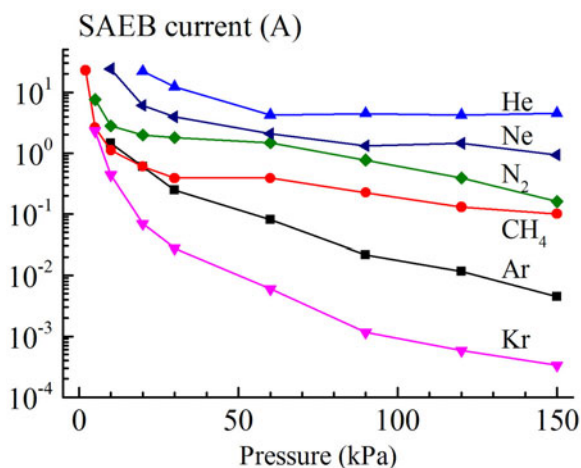


Fig. 11. SAEB current amplitude versus pressure for different gases.

time was decreased to 0.5 ns and the anode foil was made thinner, a SAEB was registered in N_2 at 0.5 MPa, in xenon and SF_6 at 0.2 MPa, and in He at 1.5 MPa; see also (Baksht *et al.*, 2008b, Zhang *et al.*, 2014). Note that in heavy gases, the ionization and excitation cross-sections are larger than those in light gases (He, H_2), which decreases the number of REs downstream of an anode.

Figure 12 shows the SAEB current amplitude against the pressure of air, N_2 , and SF_6 for different gap widths and anode foil thicknesses.

The data of collector measurements demonstrate the presence of REs downstream of the anode foil in N_2 , air, and SF_6 at pressures of several atmospheres. The number of electrons in the beam increases when using thin foils with low-electron absorption and gaps of optimum width for each gas. All data presented above were obtained on the RADAN-220 pulser. The presence of REs at pressures above 0.1 MPa was also detected by a collector in experiments on the SINUS pulser at a voltage amplitude of 180 kV and rise time of 0.5 ns (Alekseev *et al.*, 2003; Tarasenko *et al.*, 2003b). In helium, the presence of a SAEB was detected at 0.6 MPa; measurements at higher pressures were not taken due to limited strength of the working chamber. In N_2 it was detected at 0.4 MPa. At higher pressures, the presence of REs in the discharge gap could be judged from luminescence of lumino-phore downstream of the anode foil.

In most experimental conditions, the SAEB current amplitude decreases with increasing pressure. However, with certain gas-filled diode and cathode designs and certain voltage pulse parameters, a different situation may arise. For example, an increase in SAEB current amplitude with increasing the He pressure from 0.1 to 0.3–0.4 MPa was observed (Baksht *et al.*, 2008b). In this pressure range, a larger number of cathode spots were formed, as was evidenced by images of the discharge and cathode plasma glow. Likely, it was the increase in cathode spots and associated increase in emission current from the cathode, which

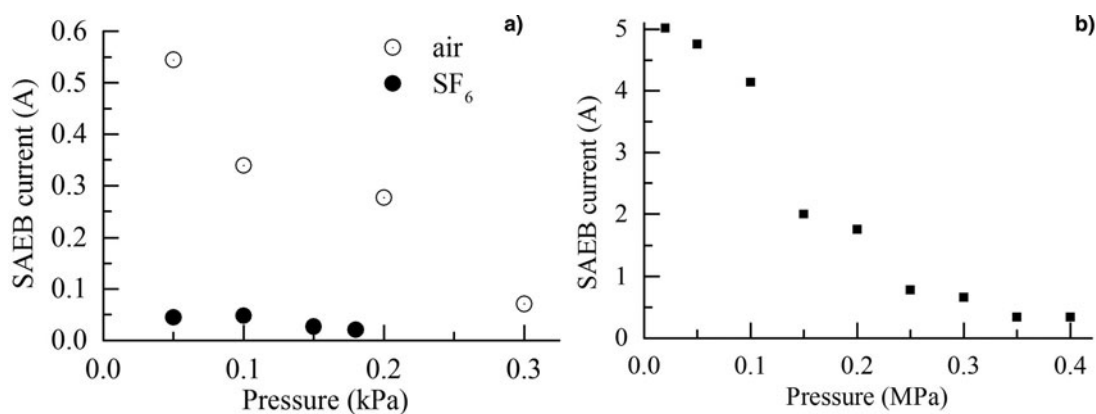


Fig. 12. SAEB current amplitude versus pressure for different gases. The SAEB was detected by a 20-mm-collector located behind a grid anode with 64% transparency and foil: (a) – air and SF₆, Al foil 10 μm thick, $d = 8$ mm; (b) – N₂, plated ketoprofen film 2 μm thick downstream of grid anode, $d = 12$ mm. Values for SF₆ are multiplied by 100.

was responsible for the buildup of SAEB currents with increasing the He pressure to 0.3–0.4 MPa.

On the RADAN-220 pulser at negative voltage polarity, an RF-3 film placed in a black paper envelope downstream of the AlMg foil was also used for the SAEB detection. A single pulse was sufficient to obtain a SAEB imprint on the RF-3 film. The highest degree of film blackening was observed in the region near the discharge gap axis. The X-ray exposure dose at an air pressure of 0.1 MPa and interelectrode gap of 13 mm was 0.6 mR. This value was the average per pulse in a series of 50 pulses. For measuring the X-ray exposure dose, the collector was removed and the AlMg foil was replaced by a Cu foil 20 μm thick. The dosimeter in these measurements was located 5 mm away from the foil. The X rays were also judged from imprints left on the film for which an additional electron absorption filter was used. Because the film sensitivity to X rays was much lower than that to electrons, more than 100 pulses were required to obtain an X-ray imprint.

At positive voltage polarity, the REs moved toward the tubular anode and hence no SAEB was detected by the collector. Also no X rays were detected by the dosimeter even after 1000 pulses when the interelectrode gap was 13 mm. Detection of X rays at positive voltage polarity was possible, as before (Shao *et al.*, 2011), only from imprints on the RF-3 film for the interelectrode gap decreased to fractions of a millimeter. However, about 10^3 pulses were required to obtain an X-ray imprint.

In the experiments described above, the discharge was diffuse but became constricted with increasing the pressure and/or with decreasing the interelectrode gap. A detailed description of spatial discharge forms and their sequence is presented in (Tarasenko, 2014). From the data reported here and in other studies (Alekseev *et al.*, 2005; Baksht *et al.*, 2008b; Tarasenko *et al.*, 2008a; Shao *et al.*, 2011, 2014; Levko *et al.*, 2012; Tarasenko, 2014; Lomaev *et al.*, 2015), it follows that it is the REs, which provide

preionization of the discharge gap and formation of a REP DD (Tarasenko, 2014).

4. ON THE MECHANISM OF RE GENERATION

Time-resolved studies of the amplitude–temporal characteristics of the RE beams generated during subnanosecond breakdowns in atmospheric-pressure gases, as well as the ones of the voltage and discharge current pulses, allow one to better understand the mechanism of RE generation in atmospheric-pressure air.

The fact of detection of the dynamic displacement current at the front of the voltage pulse indicates that electrons emission from the cathode begins with a time delay of ≤ 250 ps and a dense plasma the front of which propagates toward the anode are produced in the gap. The critical field for the appearance of field-emission electrons in vacuum is higher than 10^7 V/cm (Fursey, 2005), while the critical field for electrons to pass into the runaway mode in atmospheric-pressure nitrogen, according to the non-local criterion (Yakovlenko, 2007), is about one order of magnitude lower. Therefore, the first REs appear near the cathode with a small curvature radius immediately after the first electrons have been emitted from the cathode. If the main groups of REs registered by the collector are formed from the first electrons, then the time during which the first REs cross the discharge gap can be found from the time delay between moments of the appearance of the dynamic displacement current and the exit of SAEB electrons from the foil. In these experiments, this time was 100–200 ps. This experimental result can be compared with the calculated time during which an electron with an initial energy of 1 keV and a final energy of 100–200 keV crosses the gap with a static electric field in the collisionless mode. According to calculations, an electron with a final energy of 100 keV crosses a 1-cm-long gap over 140 ps, while that with a final energy of 200 keV, over $\cong 100$ ps. Agreement between the experimentally

determined time of flight of electrons through the 1-cm-long gap in atmospheric-pressure nitrogen and the time required for the ionization wave to cross this gap, which according to our measurements (Tarasenko *et al.*, 2015) is also 100–200 ps, confirms the mechanism of SAEB generation proposed in (Tarasenko *et al.*, 2003a). According to this mechanism, most REs are generated after the formation of dense plasma near the cathode, during propagation of the ionization wave from the cathode to the anode. Generation of most REs during the propagation of the ionization wave was substantiated in (Tarasenko *et al.*, 2008a, 2015; Tarasenko, 2011). This mechanism is also confirmed by the simultaneous detection of the dynamic displacement current and the SAEB current.

The obtained results allow us to assume that electrons with final energies of several tens of keV near the anode are generated mainly when the front of the dense plasma approaches the anode. If these electrons gained energy near the cathode, then electrons with final energies of 20 keV would pass through the gap without collisions over a time of about 300 ps and the waveforms of the beam current would exhibit an increase in the trailing edge of the SAEB pulse. However, in the waveforms of the SAEB current collected from a considerable area of the anode foil (see Fig. 9d, and 9e), the leading and trailing edges of the current pulses have nearly the same duration. An extension of the trailing edge of the current pulse is observed during registration of the fraction of the SAEB electrons that passed through a collimator with a 1-mm-diameter hole (see Fig. 7b and 9b). Such an extension of the trailing edge of the SAEB current pulse in Figure 7b and 9b can be explained by relatively slow electrons (with energies of several tens of keV), which pass into the runaway mode at a larger distance from the cathode, arriving at the collector with a certain time delay.

5. CONCLUSIONS

The results of time-resolved measurements of the amplitude–temporal characteristics of RE beams generated during subnanosecond breakdowns in atmospheric-pressure gases, as well as of the ones of the voltage and discharge current pulses, allow us to draw the following conclusions.

- (1) Registration (at using a grid anode with a especially selected transparency and cell size) of the displacement current of a “cold” diode (which means that there is no dense plasma in the gap) and the dynamic displacement current (the charging current of a “compressing capacitor” formed by the flat anode and the front of the dense plasma propagating through the gap), along with registration of the SAEB current by using a collector, make it possible to synchronize the SAEB current pulses with the waveforms of the voltage and discharge current pulses with an accuracy of several tens of picoseconds.
- (2) In atmospheric-pressure air and nitrogen at voltage pulse amplitudes of several hundred kV, the FWHM of the SAEB current pulse behind the entire surface of the anode foil is $\cong 100$ ps. When recording the SAEB current behind a small-hole collimator, it is possible to separate out a fraction of the RE beam and reduce the FWHM of the SAEB current pulse to $\cong 20$ ps. SAEB pulses are promising as a means for testing of the registration systems and collectors.
- (3) The energy spectrum of the RE beam generated during a subnanosecond breakdown consists of two to three groups of electrons with different energies. The number of electrons in the third group (electrons with the energies of higher than eU_m) does not exceed 10% of the total number of SAEB electrons.
- (4) The picosecond structure of SAEB pulses (the presence of two or more peaks spaced in time for several tens of picoseconds) registered behind small-hole collimators is caused by the non-uniformity of electron emission from different regions of the cathode during the formation of diffuse jets propagating through the discharge gap.
- (5) Double-peak SAEB pulses are generated when the gap breakdown occurs via the propagation of two ionization waves starting from the cathode.
- (6) The maximum pressure at which a SAEB is detectable decreases with increasing the voltage rise time, and for reliable SAEB detection at pressures above 0.1 MPa, one should use voltage pulses with an amplitude of 100 keV and rise time shorter than 1 ns.

ACKNOWLEDGMENTS

We are grateful to I.D. Kostyrya and D.V. Rybka for their help in performing these experiments. The work on this paper was supported by the Russian Science Foundation (Project no. 14-29-00052).

REFERENCES

- ALEKSEEV, S.B., ORLOVSKII, V.M. & TARASENKO, V.F. (2003). Electron beams formed in a diode filled with air or nitrogen at atmospheric pressure. *Tech. Phys. Lett.* **29**, 411–413.
- ALEKSEEV, S.B., ORLOVSKII, V.M., TARASENKO, V.F., TKACHEV, A.N. & YAKOVLENKO, S.I. (2005). Electron beam formation in a gas diode at high pressures. *Tech. Phys.* **50**, 1623–1627.
- BABICH, L.P. (2003). *High-Energy Phenomena in Electric Discharges in Dense Gases: Theory, Experiment, and Natural Phenomena*. Arlington, VA, USA: Published by Futurepast.
- BABICH, L.P. & LOIKO, T.V. (2010). Peculiarities of detecting pulses of runaway electrons and X-rays generated by high-voltage nanosecond discharges in open atmosphere. *Plasma Phys. Rep.* **36**, 263–270.
- BABICH, L.P. & LOIKO, T.V. (2015). Whether abnormal energy electrons are being produced in electric discharges in dense gases? *J. Exp. Theor. Phys. Lett.* **101**, 735–739.

- BAKSHT, E.KH., BURACHENKO, A.G., EROFEEV, M.V. & TARASENKO, V.F. (2014). Pulse periodic generation of supershort avalanche electron beams and X-ray emission. *Plasma Phys. Rep.* **40**, 404–411.
- BAKSHT, E.KH., BURACHENKO, A.G., KOZHEVNIKOV, V.YU., KOZYREV, A.V., KOSTYRYA, I.D. & TARASENKO, V.F. (2010). Spectrum of fast electrons in a subnanosecond breakdown of air-filled diodes at atmospheric pressure. *J. Phys. D: Appl. Phys.* **43**, 305201.
- BAKSHT, E.KH., BURACHENKO, A.G., LOMAEV, M.I., RYBKA, D.V. & TARASENKO, V.F. (2008a). Generation of runaway electron subnanosecond pulses in nitrogen and helium at a voltage of 25 kV across the gap. *Tech. Phys.* **53**, 93–98.
- BAKSHT, E.KH., LOMAEV, M.I., RYBKA, D.V., SOROKIN, D.A. & TARASENKO, V.F. (2008b). Effect of gas pressure on amplitude and duration of electron beam current in a gas-filled diode. *Tech. Phys.* **53**, 1560–1564.
- BAKSHT, E.KH., TARASENKO, V.F., LOMAEV, M.I., RYBKA, D.V. (2007). Ultrashort electron beams generated on the flat part of a voltage pulse in nitrogen and helium, *Tech. Phys. Lett.* **33**, 373–376.
- BALZOVSKY, E.V., RYBKA, D.V. & TARASENKO, V.F. (2015). Features of recording the time profile of single picosecond pulses in the real time mode. *Instrum. Exp. Tech.* **58**, 640–645.
- BELOPLOTOV, D.V., LOMAEV, M.I., SOROKIN, D.A. & TARASENKO, V.F. (2014a). Initial stage of breakdown of a point-plane gap filled with high pressure nitrogen and SF₆. *Atmosph. Ocean. Opt.* **27**, 324–328.
- BELOPLOTOV, D.V., LOMAEV, M.I., SOROKIN, D.A. & TARASENKO, V.F. (2014b). Diffuse and spark discharges at high overvoltages in high-pressure air, nitrogen, and SF₆. *Dev. Appl. Ocean. Eng.* **3**, 39–45.
- BURACHENKO, A.G. & TARASENKO, V.F. (2010). Effect of nitrogen pressure on the energy of runaway electrons generated in a gas diode. *Tech. Phys. Lett.* **36**, 1158–1194.
- FRANKEL, S., HIGHLAND, V., SLOAN, T., VAN DYCK, O. & WALES, W. (1966). Observation of X-rays from spark discharges in a spark chamber. *Nucl. Instrum. Methods* **44**, 345–348.
- FURSEY, G.N. (2005). *Field Emission in Vacuum Microelectronics*. New York, USA: Published by Plenum.
- IVANOV, S.N. (2013). The transition of electrons to continuous acceleration mode at subnanosecond pulsed electric breakdown in high-pressure gases. *J. Phys. D: Appl. Phys.* **46**, 285201.
- KOSTYRYA, I.D., BAKSHT, E.KH. & TARASENKO, V.F. (2010). An efficient cathode for generating a super short avalanche electron beams in air at atmospheric pressure. *Instrum. Exp. Tech.* **53**, 545–548.
- KOSTYRYA, I.D., RYBKA, D.V. & TARASENKO, V.F. (2012). The amplitude and current pulse duration of a supershort avalanche electron beam in air at atmospheric pressure. *Instrum. Exp. Tech.* **55**, 72–77.
- KOSTYRYA, I.D. & TARASENKO, V.F. (2004). Formation of a volume discharge in air at atmospheric pressure upon application of nanosecond high-voltage pulses. *Rus. Phys. J.* **47**, 1314–1316.
- KOZYREV, A.V., KOZHEVNIKOV, V.YU., VOROBYEV, M.S., BAKSHT, E.KH., BURACHENKO, A.G., KOVAL, N.N. & TARASENKO, V.F. (2015). Reconstruction of electron beam energy spectra for vacuum and gas diodes. *Laser Part. Beams* **33**, 183–192.
- LEVKO, D., KRASIK, YA.E. & TARASENKO, V.F. (2012). Present status of runaway electron generation in pressurized gases during nanosecond discharges. *Int. Rev. Phys.* **6**, 165–195.
- LEVKO, D., KRASIK, YA.E., TARASENKO, V.F., RYBKA, D.V. & BURACHENKO, A.G. (2013). Temporal and spatial structure of runaway electron beam in air at atmospheric pressure. *J. Appl. Phys.* **113**, 196101.
- LOMAEV, M.I., BELOPLOTOV, D.V., TARASENKO, V.F. & SOROKIN, D.A. (2015). The breakdown features of a high-voltage nanosecond discharge initiated with runaway electrons at subnanosecond voltage pulse rise time. *IEEE Trans. Dielectr. Electr. Insul.* **22**, 1833–1840.
- LOMAEV, M.I., RYBKA, D.V., SOROKIN, D.A., TARASENKO, V.F. & KRIVONOGOVA, K.YU. (2009). Radiative characteristics of nitrogen upon excitation by volume discharge initiated by runaway electron beam. *Opt. Spectrosc.* **107**, 33–40.
- MESYATS, G.A., KOROVIN, S.D., SHARYPOV, K.A., SHPAK, V.G., SHUNAILOV, S.A. & YALANDIN, M.I. (2006). Dynamics of subnanosecond electron beam formation in gas-filled and vacuum diodes. *Tech. Phys. Lett.* **32**, 18–22.
- MESYATS, G.A., REUTOVA, A.G., SHARYPOV, K.A., SHPAK, V.G., SHUNAILOV, S.A. & YALANDIN, M.I. (2011). On the observed energy of runaway electron beams in air. *Laser Part. Beams* **29**, 425–435.
- MESYATS, G.A., SADYKOVA, A.G., SHUNAILOV, S.A., SHPAK, V.G. & YALANDIN, M.I. (2013). Control and stabilization of runaway electron emission at the delay stage of pulsed breakdown in an overvolted atmospheric gap. *IEEE Trans. Plasma Sci.* **41**, 2863–2870.
- MESYATS, G.A., SHPAK, V.G., SHUNAILOV, S.A. & YALANDIN, M.I. (2008). Electron source and acceleration regime of a picosecond electron beam in a gas-filled diode with inhomogeneous field. *Tech. Phys. Lett.* **34**, 169–173.
- MESYATS, G.A., YALANDIN, M.I., REUTOVA, A.G., SHARYPOV, K.A., SHPAK, V.G. & SHUNAILOV, S.A. (2012). Picosecond runaway electron beams in air. *Plasma Phys. Rep.* **38**, 29–45.
- RYBKA, D.V., TARASENKO, V.F., BURACHENKO, A.G. & BALZOVSKII, E.V. (2012). The temporal structure of a runaway electron beam generated in air at atmospheric pressure. *Tech. Phys. Lett.* **38**, 657–660.
- SHAO, T., TARASENKO, V.F., ZHANG, CH., BAKSHT, E.KH., YAN, P. & SHUT'KO, YU.V. (2012). Repetitive nanosecond-pulse discharge in a highly nonuniform electric field in atmospheric air: X-ray emission and runaway electron generation. *Laser Part. Beams* **30**, 369–378.
- SHAO, T., TARASENKO, V.F., ZHANG, CH., BURACHENKO, A.G., RYBKA, D.V., KOSTYRYA, I.D., LOMAEV, M.I., BAKSHT, E.KH. & YAN, P. (2013). Application of dynamic displacement current for diagnostics of subnanosecond breakdowns in an inhomogeneous electric field. *Rev. Sci. Instrum.* **84**, 053506.
- SHAO, T., TARASENKO, V.F., YANG, W., BELOPLOTOV, D.V., ZHANG, CH., LOMAEV, M.I., YAN, P. & SOROKIN, D.A. (2014). Spots on electrodes and images of a gap during pulsed discharges in an inhomogeneous electric field at elevated pressures of air, nitrogen and argon. *Plasma Sources Sci. Technol.* **23**, 054018.
- SHAO, T., ZHANG, CH., NIU, Z., YAN, P., TARASENKO, V.F., BAKSHT, E.KH., KOSTYRYA, I.D. & SHUT'KO, YU.V. (2011). Runaway electron preionized diffuse discharges in atmospheric pressure air with a point-to-plane gap in repetitive pulsed mode. *J. Appl. Phys.* **109**, 083306.
- SHARYPOV, K.A., UL'MASCULOV, M.R., SHPAK, V.G., SHUNAILOV, S.A., YALANDIN, M.I., MESYATS, G.A., & KOLOMIETS, M.D. (2014). Current waveform reconstruction from an explosively

- emissive cathode at a subnanosecond voltage front. *Rev. Sci. Instrum.* **85**, 125104.
- STANKEVICH, YU.L., & KALININ, V.G. (1967). Fast electrons and X-ray radiation during the initial stage of growth of a pulsed spark. *Sov. Phys. – Dokl.* **12**, 1042–1043.
- TABATA, T. & ITO, R. (1975). A generalized empirical equation for the transmission coefficient of electrons. *Nucl. Instrum. Methods* **127**, 429–434.
- TARASENKO, V.F. (2011). Parameters of a supershort avalanche electron beam generated in atmospheric-pressure air. *Plasma Phys. Rep.* **37**, 409–421.
- TARASENKO, V.F. (Eds). (2014). *Runaway Electron Preionized Diffuse Discharges*. New York, USA: Published by Nova Science Publishers, Inc.
- TARASENKO, V.F., BAKSHT, E.KH., BURACHENKO, A.G. & EROFEEV, M.V. (2013b). Formation of diffuse and spark discharges in non-uniform electric field in elevated pressure gases. *High Volt. Eng.* **39**, 2105–2111.
- TARASENKO, V.F., BAKSHT, E.KH., BURACHENKO, A.G., KOSTYRYA, I.D., LOMAEV, M.I., PETIN, V.K., RYBKA, D.V. & SHLYAKHTUN, S.V. (2008c). Energy distribution of runaway electrons generated by a nanosecond discharge in atmospheric-pressure air. *Plasma Phys. Rep.* **34**, 1028–1036.
- TARASENKO, V.F., BAKSHT, E.KH., BURACHENKO, A.G., KOSTYRYA, I.D., LOMAEV, M.I. & RYBKA, D.V. (2010a). High-pressure runaway-electron – preionized diffuse discharges in a nonuniform electric field. *Tech. Phys.* **55**, 210–218.
- TARASENKO, V.F., BAKSHT, E.KH., BURACHENKO, A.G., KOSTYRYA, I.D., LOMAEV, M.I. & RYBKA, D.V. (2008a). Generation of supershort avalanche electron beams and formation of diffuse discharges in different gases at high pressure. *Plasma Dev. Oper.* **16**, 267–298.
- TARASENKO, V.F., BAKSHT, E.KH., BURACHENKO, A.G., KOSTYRYA, I.D., LOMAEV, M.I. & RYBKA, D.V. (2008b). Supershort avalanche electron beam generation in gases. *Laser. Part. Beams* **26**, 605–617.
- TARASENKO, V.F., BAKSHT, E.KH., BURACHENKO, A.G., KOSTYRYA, I.D. & RYBKA, D.V. (2013a). Energy of electrons generated during a subnanosecond breakdown in atmospheric-pressure air. *Plasma Phys. Rep.* **39**, 592–599.
- TARASENKO, V.F., BAKSHT, E.KH., BURACHENKO, A.G., LOMAEV, M.I., SOROKIN, D.A. & SHUT'KO, YU.V. (2010b). On the initiation of a spark discharge upon the breakdown of nitrogen and air in a non-uniform electric field. *Tech. Phys.* **55**, 904–907.
- TARASENKO, V.F., BELOPLOTOV, D.V. & LOMAEV, M.I. (2015). Dynamics of ionization processes in high-pressure nitrogen, air, and SF₆ during a subnanosecond breakdown initiated by runaway electrons. *Plasma Phys. Rep.* **41**, 832–846.
- TARASENKO, V.F., BURACHENKO, A.G., BAKSHT, E.KH., KOSTYRYA, I.D., LOMAEV, M.I. & RYBKA, D.V. (2009). A coaxial chopping gap filled with air at atmospheric pressure with a pulse decay time ≤ 100 ps. *Instrum. Exp. Tech.* **52**, 366–369.
- TARASENKO, V.F., EROFEEV, M.V., LOMAEV, M.I., SOROKIN, D.A. & RYBKA, D.V. (2012a). Two component structure of the current pulse of runaway electron beam generated during electron breakdown of elevated pressure nitrogen. *Plasma Phys. Rep.* **38**, 922–929.
- TARASENKO, V.F., ORLOVSKII, V.M. & SHUNAILOV, S.A. (2003a). Forming of an electron beam and a volume discharge in air at atmospheric pressure. *Rus. Phys. J.* **46**, 325–327.
- TARASENKO, V.F., RYBKA, D.V., BURACHENKO, A.G., LOMAEV, M.I. & BALZOVSKY, E.V. (2012b). Measurement of extreme-short current pulse duration of runaway electron beam in atmospheric pressure air. *Rev. Sci. Instrum.* **83**, 086106.
- TARASENKO, V.F., SHPAK, V.G., SHUNAILOV, S.A. & KOSTYRYA, I.D. (2005). Supershort electron beam from air filled diode at atmospheric pressure. *Laser Part. Beams* **23**, 545–551.
- TARASENKO, V.F., YAKOVLENKO, S.I., ORLOVSKII, V.M., TKACHEV, A.N. & SHUNAILOV, C.A. (2003b). Production of powerful electron beams in dense gases. *JETP Lett.* **77**, 611–615.
- TARASOVA, L.V. & KHUDYAKOVA, L.N. (1969). X-Rays from pulsed discharges in air. *Sov. Phys. Tech. Phys.* **14**, 1148–1150.
- TARASOVA, L.V., KHUDYAKOVA, L.N., LOIKO, T.V. & TSUKERMAN, V.A. (1974). The fast electrons and X-ray radiation of nanosecond pulsed discharges in gases under 0.1–760 Torr. *J. Tech. Phys.* **44**, 564–568.
- WILSON, C.T.R. (1924). The acceleration of β -particles in strong electric fields such as those of thunderclouds. *Proc. Camb. Philos. Soc.* **22**, 534–538.
- YAKOVLENKO, S.I. (Eds). (2007). *Beams of Runaway Electrons and Discharges in Dense Gases, Based on a Wave of Multiplication of Background Electrons*. Moscow, Russia: Published by Nauka. [in Russian].
- YALANDIN, M.I., REUTOVA, A.G., SHARUPOV, K.A., SHPAK, V.G., SHUNAILOV, S.A., UL'MACULOV, M.R., ROSTOV, V.V. & MESYATS, G.A. (2010). Stability of injection of a subnanosecond high-current electron beam and dynamic effects within its rise time. *IEEE Trans. Plasma Sci.* **38**, 2559–2564.
- ZAGULOV, F.YA., KOTOV, A.S., SHPAK, V.G., YURIKE, YA. YA. & YALANDIN, M.I. (1989). RADAN – small-size pulse-periodic high-current accelerator of electrons. *Prib. Tekh. Eksp.* **2**, 146–149.
- ZHANG, CH., TARASENKO, V., GU, J., BAKSHT, E., WANG, R., YAN, P. & SHAO, T. (2015). A comparison between spectra of runaway electron beams in SF₆ and air. *Phys. Plasmas* **22**, 123516.
- ZHANG, CH., TARASENKO, V.F., SHAO, T., BAKSHT, E.KH., BURACHENKO, A.G., YAN, P. & KOSTYRYA, I.D. (2013). Effect of cathode materials on the generation of runaway electron beams and X-rays in atmospheric pressure air. *Laser Part. Beams* **31**, 353–364.
- ZHANG, CH., TARASENKO, V.F., SHAO, T., BELOPLOTOV, D.V., LOMAEV, M.I., SOROKIN, D.A. & YAN, P. (2014). Generation of supershort avalanche electron beams in SF₆. *Laser Part. Beams* **32**, 331–341.